PHYSICAL REVIEW APPLIED **11,** 014050 (2019)

Seebeck Coefficient of $\mathrm{Au}_x\mathrm{Ge}_{1-x}$ Thin Films Close to the Metal-Insulator Transition for Molecular Junctions

C. Salhani, J. Rastikian, C. Barraud, P. Lafarge, and M. L. Della Rocca[*]
Laboratoire MPQ, Université Paris Diderot, Sorbonne Paris Cité, UMR 7162, CNRS, 10 rue Alice Domon et Léonie Duquet, 75205 Paris Cedex 13, France

(Received 24 June 2018; revised manuscript received 6 November 2018; published 25 January 2019)

We experimentally study the thermoelectric properties of an $\mathrm{Au}_x\mathrm{Ge}_{1-x}$ thin-film alloy close to the metal-insulator transition ($x = 19.5\%$). The thermoelectric characterization of the thin-film alloy shows a Seebeck coefficient comparable to that of Au thin film while preserving good thermal sensor properties, revealing the potential interest in its use in nanoscale thermoelectric systems. In particular, we demonstrate the ability to directly evaporate an $\mathrm{Au}_x\mathrm{Ge}_{1-x}$ thin film on different nanometric-thick molecular layers. A device engineering is proposed paving the way for investigation of the thermoelectricity of large-area nanometric-thick molecular layers, where the alloy is integrated as a contact electrode, fulfilling the double role of an *in situ* local heater and a high-resolution thermometer.

DOI: 10.1103/PhysRevApplied.11.014050

I. INTRODUCTION

Thermal transport at the nanoscale has recently been the subject of renewed interest both theoretically and experimentally, due to the ability to tailor the electronic properties of materials by quantum design [1,2]. In particular, exciting results have been achieved in the field of molecular thermoelectricity. Following the pioneering work of Reddy *et al.* [3], recent experiments have reported combined conductance and thermopower measurements [4–6], gate control of thermoelectric effects [7], Peltier cooling of molecular junctions [8], the influence of the mechanical-junction configuration on thermoelectricity [9], and an enhanced thermoelectric effect in cross-conjugated molecules [10–12]. However, most results in this field have been obtained on systems consisting of single or few molecules, whereas the thermoelectric properties of large-area molecular junctions remain unexplored. Such junctions are good candidates for potential applications of molecular electronics owing to a complementary-metal-oxide-semiconductor- (CMOS-) compatible fabrication process and a high robustness [13–16]. In any event, contacting large-area molecular junctions is a longstanding issue. Direct evaporation of a metal electrode on a few-nanometer-thick molecular layer usually ends up with the formation of short circuits due to the presence of metallic filaments. This has led to the development of multiple approaches (conducting atomic-force microscopy, Ga-In eutectic contact), which are typically not compatible with applications. The successful integration of aromatic molecules in large-area molecular junctions by the electroreduction of diazonium salt has represented an important breakthrough [14–17]. Such a technique allows the realization of a thin and robust molecular layer covalently grafted onto a surface electrode and able to sustain the direct evaporation of a counter-electrode in a cross-bar geometry. Recently, junctions based on various molecules have been successfully fabricated with Ti/Au, Cu, and electron-beam evaporated carbon top electrodes [14–19]. However, this molecular junction architecture has never been tested for thermoelectric investigation because of the difficulty of achieving a thermal gradient across it. The use of CMOS-compatible fabrication methods with organic molecules, where a possible high thermoelectric efficiency can be achieved [11,20], could represent a new route for energy-harvesting applications at the nanoscale. In any event, probing the thermopower of large-area molecular junctions requires the current through the junctions to be measured while simultaneously heating only one of the contacts and measuring the temperature difference across the junction *in situ*. This cannot be achieved with Au or e-carbon contacts, due to low and high resistivity, respectively. Furthermore, another general issue in realizing thermoelectric measurements is to reduce any spurious thermoelectric signal, such as that related to the junction electrodes in the case of a large-area molecular junction, as much as possible. As a consequence, the device design and the choice of materials for exploring the thermoelectricity of molecular films are crucial aspects that need to be investigated in detail.

Here, we report on the growth and thermoelectric characterization of $\mathrm{Au}_x\mathrm{Ge}_{1-x}$ thin-film alloys ($x = 19.5\%$) and

---

[*] maria-luisa.della-rocca@univ-paris-diderot.fr

on the fabrication of large-area molecular junctions with a $\mathrm{Au}_x\mathrm{Ge}_{1-x}$ top contact. We discover that for this particular composition, placing the alloy close to its metal-insulator transition (MIT) [21–24], the Seebeck coefficient is very close to that of pure Au films up to 200 K, while the alloy preserves good thermosensor properties. This aspect is particularly appealing for thermoelectric applications. We demonstrate, therefore, the possibility of directly depositing the alloy on a nanometric-thick molecular layer covalently bonded onto a gold electrode, in order to achieve a large-area molecular junction in a cross-bar configuration. A $\mathrm{Au}_x\mathrm{Ge}_{1-x}$-based junction electrode with such a low Seebeck coefficient can fulfill the double requirement of being resistive enough to generate Joule heating and having a resistance that is sensitive enough to temperature to be used as a local thermometer, opening up new perspectives for molecular thermoelectricity.

More generally, our findings encourage the use of such thin-film alloys as heaters and thermosensors in nanoscale devices designed to investigate the thermoelectric properties of low-dimensional materials such as nanowires [25–28], graphene [29,30], and carbon nanotubes [31,32], where metal-based nanowires with lower sensitivity are typically used.

II. SAMPLE FABRICATION AND METHODS

The fabrication of $\mathrm{Au}_x\mathrm{Ge}_{1-x}$ thin-film alloys is realized following Zhu *et al.* [24], who take advantage of the interfacial atomic-diffusion mechanism of Au and Ge atoms occurring in a superlattice configuration. Thin films with an optical-lithography-defined area of $50 \times 150\ \mu\mathrm{m}^2$ and a thickness of 100 nm are obtained in a superlattice structure by alternating the evaporation of 1 nm of Au (Neyco, 99.99%) and 6 nm of Ge (Neyco, 99.99%) at low rates (0.01 and 0.05 nm/s, respectively) on $\mathrm{Si}/\mathrm{SiO}_2$ substrates at room temperature (the Si substrate is boron doped, with a resistivity of $\rho_{\mathrm{Si}} \simeq 0.2$–$0.4\ \Omega\mathrm{cm}$ at room temperature). The base pressure of the evaporation chamber is approximately 5×10^{-8} mbar and increases to approximately 1×10^{-7} mbar during processing. A quartz crystal is used to monitor the thicknesses of the layers and the atomic rates. The ratio between the thicknesses of the Ge and Au layers is chosen to reach a composition close to the metal-insulator transition, which occurs around $x = 18\%$. After evaporation, samples are left in the vacuum chamber overnight. A subsequent optical-lithography step defines four Ni/Au (10 nm/300 nm) contact probes for electrical characterization. The use of a Ni adhesion layer helps in the formation of ohmic contacts with the $\mathrm{Au}_x\mathrm{Ge}_{1-x}$ alloy [33] and the Au capping layer allows easy wire bonding. Finally, in order to promote alloy formation with a stable film resistance, a 24 h annealing at 135 °C is realized [34]. A long-time low-temperature annealing is preferred to a short-time high-temperature one so as to obtain the formation of the alloy by a process that can be compatible with the presence of a molecular layer. As we will discuss later, the whole thin-film alloy fabrication procedure is well matched for the integration of this material as one electrode of a large-area junction including a molecular layer.

Figure 1(a) shows a schematic representation of the device and a scanning-electron-microscope (SEM) image of the final device is reported in Fig. 1(b). The four Ni/Au contacts are labeled *a*, *b*, *c*, and *d*. They have a minimum width of $\simeq 10\ \mu$m and are spaced at $d_{ab} = d_{bc} = 10\ \mu$m and $d_{cd} = 70\ \mu$m from each other.

Energy-dispersive x-ray (EDX) analysis is performed in order to evaluate the average composition of the alloy. This estimation is done by averaging the spectral weight on 30 different zones of the sample. An example of some EDX spectra is reported in Fig. 2(a) in the 0–10 keV energy range, where the positions corresponding to the *K*, *L*, and *M* lines of Si, Au, and Ge can be easily identified. The quantitative analysis of line intensities allows us to determine the concentration of each element in the sample. In the case of Fig. 2(a), a thin-film alloy with an Au atomic concentration of 19.5% and a Ge atomic concentration of 80.5% is realized, confirming the achievement of a composition close to the metal-insulator transition, located

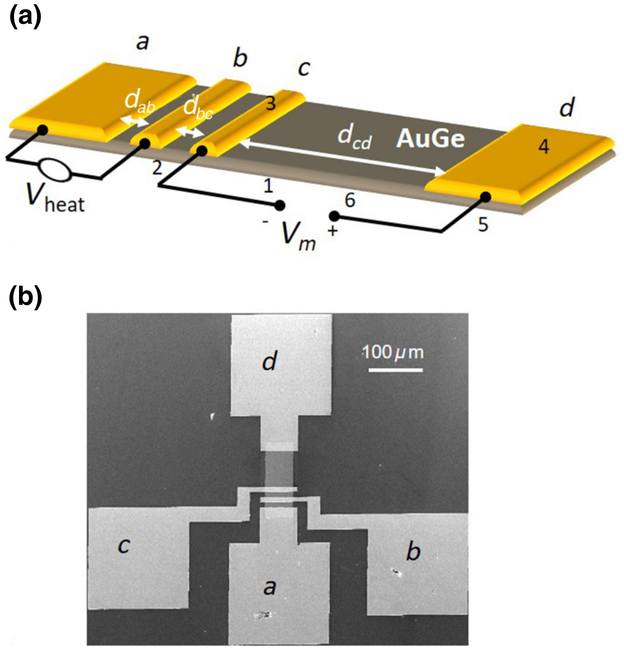

FIG. 1. (a) A schematic representation of the device. The four Ni/Au contact probes, labeled *a*, *b*, *c*, and *d*, are spaced at $d_{ab} = 10\ \mu$m, $d_{bc} = 10\ \mu$m, and $d_{cd} = 70\ \mu$m. The numbers from 1 to 6 define zones of the device with different temperatures. (b) A SEM image of a $\mathrm{Au}_x\mathrm{Ge}_{1-x}$ thin film with an area of $50 \times 150\ \mu\mathrm{m}^2$ and a thickness of 100 nm.

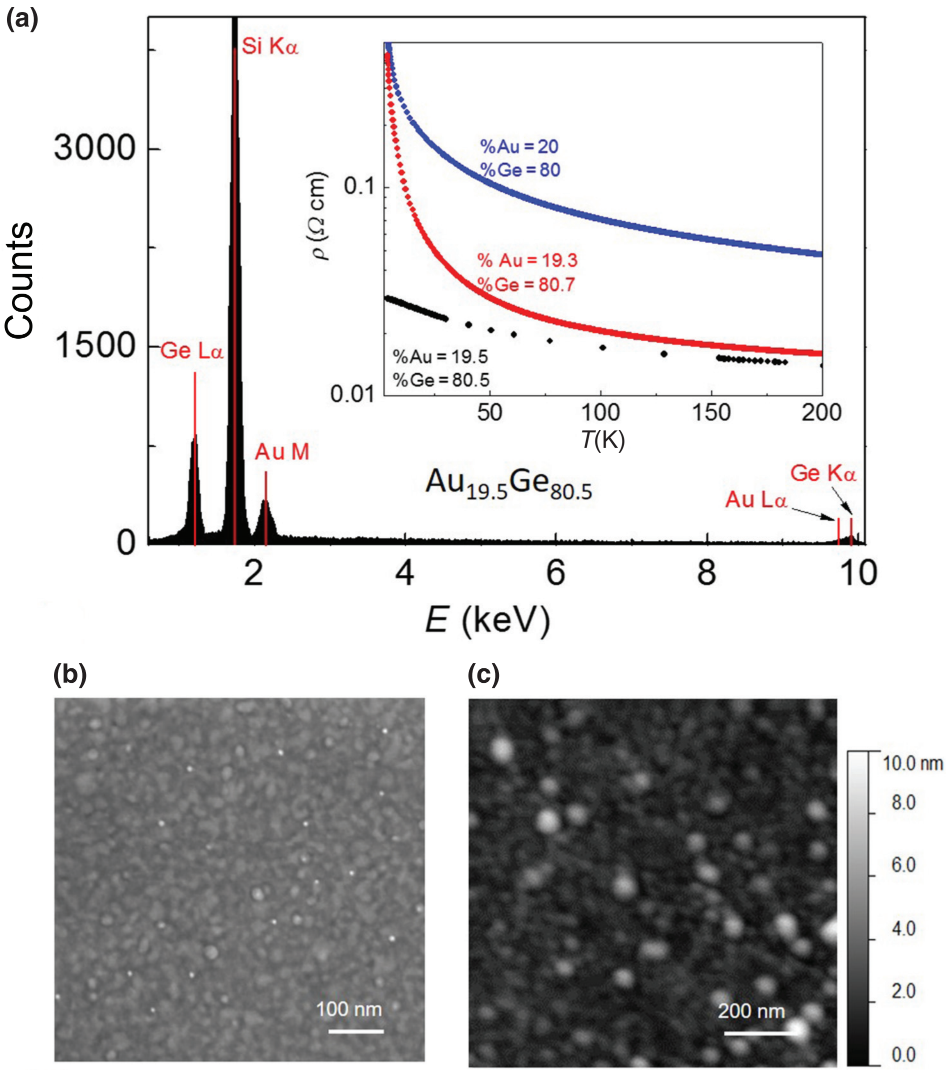

FIG. 2. (a) EDX analysis of the $\mathrm{Au}_{19.5}\mathrm{Ge}_{80.5}$ alloy. Characteristic K, L, and M lines of Au, Ge, and Si are visible. The alloy composition of $\mathrm{Au}_{80.5}\mathrm{Ge}_{19.5}$ is determined by averaging on 30 different zones. Inset: the temperature dependence of the resistivity in the range $4\ \mathrm{K} \leq T \leq 250\ \mathrm{K}$ for three samples fabricated as described in the main text but at different moments. The atomic composition in each case is indicated following the same color code as the measured curve. (b) A SEM image of the alloy surface. (c) An AFM image of the alloy surface.

slightly on the metallic side of the transition. Element-distribution maps obtained by scanning the beam in a televisionlike raster and displaying the intensity of the selected Au and Ge x-ray line confirm that the elements are well diluted within the alloy at the explored scale.

We study the morphology of the alloy surfaces by SEM or by atomic-force microscopy (AFM). Two surface images are reported in Figs. 2(b) (SEM) and 2(c) (AFM) for two different samples. The images reveal the presence of grains the dimensions of which depend on the particular sample. Figure 2(b) shows a typical grain size of 20–30 nm. Surprisingly, very small and regular grains with dimensions lower than 10 nm are visible in the SEM image as brighter spots, uniformly distributed on the surface [the white spots in Fig. 2(b)]. This can probably be attributed to aggregates of Au atoms in the alloy that are not perfectly diluted. The AFM image reveals the presence of higher grains dimensions, with a more important size dispersion, in the 10–50 nm range. Surface analysis averaged on ten different zones of the sample with an area of $3 \times 3\ \mu\mathrm{m}^2$ gives an average root-mean-square roughness of approximately 4 nm. This structural and morphological analysis reveals that repeating the same fabrication procedure exactly does not yield precisely the same atomic composition, nor exactly the same morphology of the samples. The inset of Fig. 2(a) shows the temperature dependence of the resistivity between $4\ \mathrm{K} \leq T \leq 250\ \mathrm{K}$ for three samples fabricated under identical conditions but having different atomic concentrations. The EDX results show a dispersion in composition slightly less than approximately 1%. The resistivity versus temperature curves prove, as expected, that the electronic-transport properties are sensitive to the alloy composition [21,35] and the way in which the alloy forms. However, such a dispersion does not prevent the possibility of using the films as thermosensors, since important variations of the resistivity are present in the explored temperature range for all the samples. Hereafter, we will focus on the thermoelectric characterization of one of the samples of Fig. 2(b) showing the composition $\mathrm{Au}_{19.5}\mathrm{Ge}_{80.5}$. As explained afterwards, we expect that slightly composition oscillations affect only marginally the thermoelectric response.

The thermoelectric characterization of the alloy is realized in a cryofree refrigerator that allows temperature variation from 3.7 K to 300 K with a stability of few millikelvins. A nonlocal scheme is adopted to heat only part of the sample and to generate a temperature gradient along the longitudinal dimension of the $\mathrm{Au}_x\mathrm{Ge}_{1-x}$ thin film. A dc voltage, V_{heat}, is applied between contacts a and b, inducing power dissipation by Joule heating ($P = IV \sim \Delta T$). Even if the power dissipation takes place between contacts a and b, a lower temperature increase is also induced on contact c. Contact d is far enough from contact c to be considered as being at the temperature of the substrate, T_{env}, which is thermally anchored to the sample holder by a GE (IMI 7031) low-temperature glue (CMR-Direct). The thermal conductivity of the glue (0.24 W/m K) is lower than that of the Si substrate ($\simeq$150 W/m K) and the SiO_2 oxide layer (0.7 W/m K); this ensures that the thermalization of the sample takes place mainly through wire bonding on the metallic pads (with in-plane dimensions of $200 \times 200\ \mu\mathrm{m}^2$). A temperature sensor is fixed to the sample holder in order to have continuous monitoring of the substrate temperature.

Such a temperature-gradient scheme is supported by finite-element simulations performed with the COMSOL multiphysics software (Joule heating and conductive media modules). Figure 3 shows the result of the simulation for a $\mathrm{Au}_x\mathrm{Ge}_{1-x}$ thin film on a $\mathrm{Si/SiO}_2$ substrate with the four Ni/Au contatcs. The dimensions of the simulated device are equal to that of the fabricated one. A dc voltage drop of 2 V is simulated between contacts a and b, the voltage being applied on contact b while grounding contact a, and all surfaces are considered to be electrically insulated. The high thermal conductivity of the Ni/Au contacts and the thermal coupling to the sample holder through the connection pads and the substrate induces the thermalization of the $\mathrm{Au}_x\mathrm{Ge}_{1-x}$ thin film. The temperature of the bottom plane of the substrate, thermalized with the cold finger of the cryostat, as well as the temperature of the contacting pads, thermalized through the wire bonding to the sample holder, are fixed at the temperature of the surrounding environment. All other surfaces are considered to be insulating. The presence of the low-temperature glue thermalizing the substrate is taken into account by considering the value of the thermal conductivity at the interface between the substrate and the sample holder to be equal to 0.24 W/m K. All other thermal boundary resistances are neglected to simplify the simulations. The calculations are performed by considering the electrical and thermal properties of the different materials extracted from the literature [7] and by solving the Fourier low for heat transfer in isotropic media, $\overrightarrow{\nabla} T = -\overrightarrow{q}/k$, where $\overrightarrow{\nabla} T$ is the temperature-gradient field, $\overrightarrow{q}$ is the local heat flux, and k the thermal conductivity. Note that the only unknown parameter in the simulations is the thermal conductivity of the thin-film alloy, k_{AuGe}, which is varied over a wide range (1–150 W/m K). Note also that the simulation results are intended to produce only qualitative information.

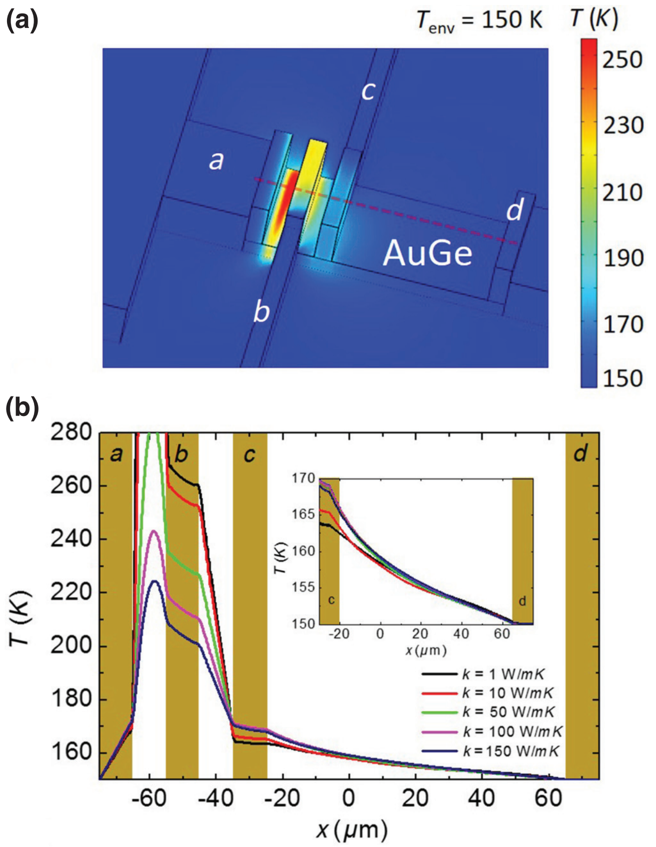

FIG. 3. (a) A three-dimensional color plot of the temperature in the $\mathrm{Au}_x\mathrm{Ge}_{1-x}$ thin-film alloy for an applied voltage V_{heat} of 2 V between contacts a and b at a temperature $T_{\mathrm{env}} = 150$ K of the surrounding environment. (b) Temperature profiles in the longitudinal direction of the device [red dotted line in (a)] calculated by varying the k_{AuGe} value from 1 to 150 W/m K. A temperature gradient of the order of 20 K develops between contacts c and d. The positions of the contact probes are indicated by the vertical dark yellow bars. Inset: an enlargement of the calculated temperature profiles between contacts c and d.

Large temperature gradients are developed for large heat fluxes and/or for low thermal conductivities. A color plot of the temperature gradient, in Fig. 3(a), shows the simulation for a temperature of the environment equal to $T_{\mathrm{env}} = 150$ K when a voltage $V_{\mathrm{heat}} = 2$ V is applied between contacts a and b. The color scale demonstrates that the maximum temperature rise is located at the $\mathrm{Au}_x\mathrm{Ge}_{1-x}$ thin-film zone between contacts a and b. This reflects the fact that the heat current in this region is high and that the thermal conductivity of $\mathrm{Au}_x\mathrm{Ge}_{1-x}$ is lower with respect to Au. However, the simulation shows that a temperature drop along the $\mathrm{Au}_x\mathrm{Ge}_{1-x}$ thin film can be developed between contacts c and d. Temperature profiles taken in the longitudinal direction of the device at the center of the thin-film alloy by varying k_{AuGe} from 1 to 150 W/m K are plotted in Fig. 3(b). The positions of the contact probes are indicated by the vertical dark yellow bars in the figure. Varying k_{AuGe} mostly affects the maximum temperature reached in the region between contacts a and b. The average temperature rise between contacts c and d when a voltage, V_{heat}, is applied between contacts a and b, is not greatly affected by the value of k_{AuGe} [see the inset to Fig. 3(b)]. This indicates that the heat flow should be dominated by the substrate, which has the highest heat conductance in the system since it is 3 orders of magnitude thicker than the other components of the device. From the simulation, we can conclude that the temperature gradient between contacts c and d can be considered at a first approximation as a linear function of the distance, regardless of the value of k_{AuGe}. Qualitative knowledge of the expected temperature profile as a function of the distance between contacts c and d allows us to extract the real temperature gradient developed in this region, as will be explained in the next section.

In order to extract the real temperature in the different parts of the thin-film alloy, calibration curves are realized consisting in the measurement of the resistances between the different electrical contacts, R_{ab}, R_{bc}, and R_{cd}, as a function of the temperature of the environment. The resistances are measured using the standard ac technique, by applying an ac voltage of low amplitude at low frequency ($V_{\mathrm{ac}} = 1\,\mathrm{mV}$, $f \simeq 17\,\mathrm{Hz}$) and by measuring the resulting ac current using a low-noise current-voltage amplifier. With the help of these calibrations, we can extract the average temperature rise between any pair of contacts when a dc voltage is applied between any other pair. The thermoelectric scheme measurement of Fig. 1(a) is thus adopted: while heating the Au_xGe_{1-x} alloy between contacts a and b, the thermoelectric voltage between contacts c and d is simultaneously measured.

III. RESULTS AND DISCUSSION

Until now, the thermoelectric power of the Au_xGe_{1-x} thin film has only been studied at high temperature ($T > 400\,\mathrm{K}$) for different Au concentrations as a function of a thermal annealing treatment, inducing a transition from an amorphous to a recrystallized phase of the thin films [35]. Thermopowers as large as approximately 4–5 mV/K have been reported for a low Au concentration (5%) in such a temperature range even though large fluctuations are still present. A detailed characterization close to the MIT and in a lower temperature range more appropriate for studying thermoelectricity of molecular layers is therefore lacking.

We discuss here the electrical and thermoelectric characterizations of the $Au_{19.5}Ge_{80.5}$ alloy close to the MIT. We first realize calibration curves of the different segments of the thin-film alloy over a wide temperature range, as described in the previous section. A typical calibration curve is shown in the inset of Fig. 4(a), where the resistance of the ab segment, R_{ab}, is measured in the temperature range 3.7–260 K. As expected close to the metal-insulator transition of the alloy, R_{ab} increases when the temperature is lowered, leading to the realization of a good temperature sensor, particularly in the low-temperature regime.

At the base temperature of the cryostat (3.7 K), no thermoelectric voltage is detected above the noise level of our experimental setup. The measurements are thus realized at higher temperature, $T_{\mathrm{env}} = 150$ K and $T_{\mathrm{env}} = 200$ K, where a measurable signal is observed even if, in this temperature range, the sensitivity of the $Au_{19.5}Ge_{80.5}$ sensor is reduced. Figures 4(a) and 4(c) show the calibration curves of the thermoelectric source of the $Au_{19.5}Ge_{80.5}$ thin-film alloy, corresponding to the resistance of the cd segment, R_{cd}, in the temperature ranges 150–185 K [Fig. 4(a)] and 200–260 K [Fig. 4(c)]. In the two explored temperature ranges, the R_{cd} variation allows us to monitor the temperature with a resolution of 3.7 Ω/K and 2.5 Ω/K, respectively. A linear fit of the calibration curves (the solid red lines) shows a temperature dependence of the form $R_{cd} = R_0(1 + \alpha T)$, where α is a negative temperature coefficient. We find $R_0 = 1806 \pm 3\ \Omega$ and $\alpha = -2.03 \times 10^{-3} \pm 1\ \times 10^{-5}\,\mathrm{K}^{-1}$ at $T_{\mathrm{env}} = 150\,\mathrm{K}$ [Fig. 4(a)] and $R_0 = 1583 \pm 5\,\Omega$ and $\alpha = -1.58 \times 10^{-3} \pm 2\ \times 10^{-5}\,\mathrm{K}^{-1}$ at $T_{\mathrm{env}} = 200\,\mathrm{K}$ [Fig. 4(b)], respectively. The calibration curves allow the power dissipated by an applied dc voltage in the ab segment, V_{heat}, to be converted in the temperature gradient along the cd segment as explained in what follows. Based on the finite-element simulation shown above, we assume in a first approximation that the temperature gradient between contacts c and d has a linear dependence on the distance x: $T(x) = T_c - (T_c - T_d)x/d_{cd}$. A straightforward calculation shows that $\Delta T_{cd} = T_c - T_d$ can be expressed as a function of the applied voltage V_{heat} as follows:

$$\Delta T_{cd}(V_{\mathrm{heat}}) = \frac{2\Delta R(V_{\mathrm{heat}})}{\alpha R_0}, \tag{1}$$

where $\Delta R(V_{\mathrm{heat}}) = R_{cd}(V_{\mathrm{heat}}) - R_{cd}(V_{\mathrm{heat}} = 0)$, in which $R_{cd}(V_{\mathrm{heat}})$ is the resistance between contacts c and d when a dc voltage V_{heat} is applied between contacts a and b. The parameters α and R_0 are extracted from the fit of the calibration curves shown in Figs. 4(a) and 4(c). The insets of Figs. 4(b) and 4(d) show ΔT_{cd} as a function of V_{heat} in the range $-2\,\mathrm{V} \le V_{\mathrm{heat}} \le 2\,\mathrm{V}$ for a temperature of the environment of $T_{\mathrm{env}} = 150\,\mathrm{K}$ and $T_{\mathrm{env}} = 200\,\mathrm{K}$, respectively. As expected, the curves show a paraboliclike behavior verified by the fitting given by the solid red curves.

The central result of the paper is represented in the main panel of Figs. 4(b) and 4(d), where the thermoelectric

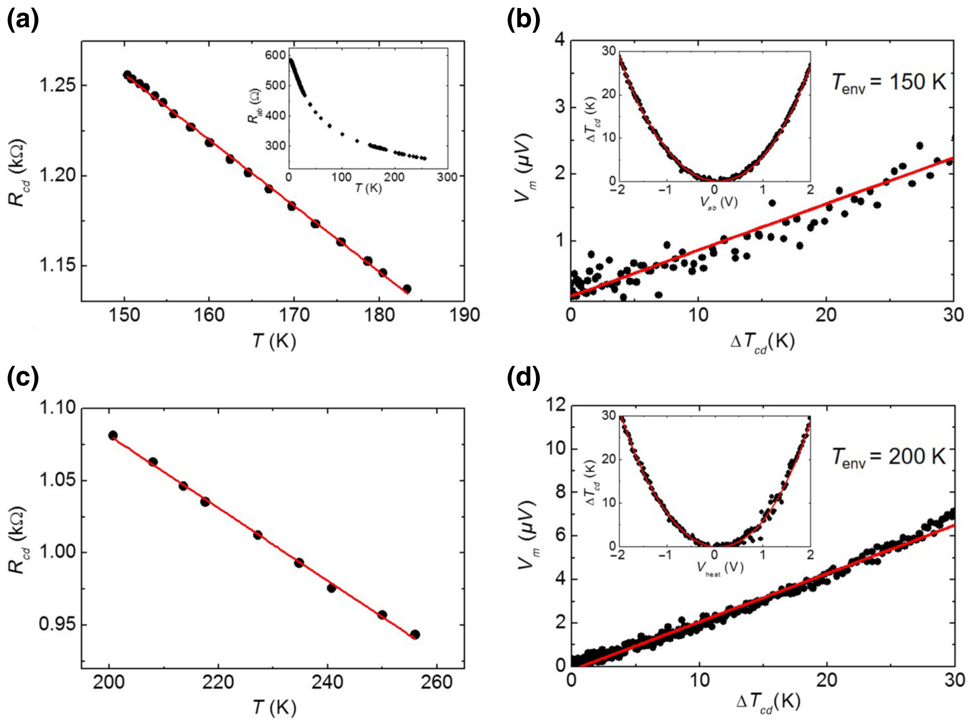

FIG. 4. (a) The temperature dependence of the resistance of the *cd* segment, R_{cd}, of the $\mathrm{Au}_{19.5}\mathrm{Ge}_{80.5}$ thin-film alloy in the range 150–185 K. Inset: the resistance of the *ab* segment, R_{ab}, measured in the temperature range 3.7–260 K. (b) The thermoelectric voltage measured on the *cd* segment of the $\mathrm{Au}_{19.5}\mathrm{Ge}_{80.5}$ thin-film alloy heated following a nonlocal scheme at a temperature of the environment of $T_{\mathrm{env}} = 150\,\mathrm{K}$. Inset: the temperature increase ΔT_{cd} between contacts *c* and *d* when applying a dc voltage V_{heat} between contacts *a* and *b*. (c) The temperature dependence of the resistance of the *cd* segment, R_{cd}, of the $\mathrm{Au}_{19.5}\mathrm{Ge}_{80.5}$ thin-film alloy in the range 200–260 K. (d) The thermoelectric voltage measured on the *cd* segment of the $\mathrm{Au}_{19.5}\mathrm{Ge}_{80.5}$ thin-film alloy heated following a nonlocal scheme at a temperature of the environment of $T_{\mathrm{env}} = 200\,\mathrm{K}$. Inset: the temperature increase ΔT_{cd} between contacts *c* and *d* when applying a dc voltage V_{heat} between contacts *a* and *b*. In all of the figures, the black dots are the experimental data and the solid red lines are fitting curves.

voltage V_m measured on the *cd* segment of the $\mathrm{Au}_{19.5}\mathrm{Ge}_{80.5}$ thin-film alloy is plotted as a function of ΔT_{cd}. The experimental points follow a linear behavior for ΔT_{cd} in the 0–30 K. Note that the experimental data correspond to measurements taken with both signs of the polarization voltage. This proves that the sign of the thermoelectric signal is independent of the direction of the current between contacts *a* and *b*, since the same signal is measured when current flows from contact *a* to contact *b* and from contact *b* to contact *a*. Following the schematic representation of Fig. 1(a), the measured Seebeck coefficient, S_m, defined as $S_m = -[(V_1 - V_6)/(T_3 - T_4)] = -\Delta V_{16}/\Delta T_{34}$, can be evaluated from the slope of the linear trend of the experimental data. Note that we measure experimentally the potential difference $V_m = V_6 - V_1$, which has the opposite direction with respect to the temperature gradient, defined by $\Delta T_{cd} = T_c - T_d = T_3 - T_4 = \Delta T_{34}$. This implies that according to the notation and to the adopted measurement conventions, the extracted Seebeck coefficient, S_m, is indeed a positive quantity. We find particularly low values of S_m, of the order of $S_m \simeq 0.069 \pm 0.006\ \mu\mathrm{V/K}$ at $T_{\mathrm{env}} = 150\,\mathrm{K}$ and $S_m \simeq 0.222 \pm 0.005\ \mu\mathrm{V/K}$ at $T_{\mathrm{env}} = 200\,\mathrm{K}$. To correctly interpret the measured thermopower values, we consider the effect of thermal gradients developed on the different parts of the device, including the connection lines to the instruments, inducing additional thermoelectric contributions. Following the schematic representation shown in Fig. 1(a), the contributions of all the different parts of the device can be written as follows:

$$
\begin{aligned}
V_2 - V_1 &= -S_{\mathrm{wire}}(T_2 - T_1),\\
V_3 - V_2 &= -S_{\mathrm{Ni/Au}}(T_3 - T_2),\\
V_4 - V_3 &= -S_{\mathrm{AuGe}}(T_4 - T_3),\\
V_5 - V_4 &= -S_{\mathrm{Ni/Au}}(T_5 - T_4),\\
V_6 - V_5 &= -S_{\mathrm{wire}}(T_6 - T_5),
\end{aligned}
$$

where S_{AuGe} is the Seebeck coefficient of the $\mathrm{Au}_{19.5}\mathrm{Ge}_{80.5}$ thin-film alloy, S_{wire} is the Seebeck coefficient of the connection lines in the cryostat, $S_{\mathrm{Ni/Au}}$ is the Seebeck coefficient of the Ni/Au thin-film contact probes, and V_i and T_i (with $i = 1, 6$) are the voltage and the temperature at each point indicated in the inset of Fig. 1(a).

By adding the five equations and by taking into account that $T_1 = T_6 = T_{rt}$ with T_{rt} the room temperature, $T_2 = T_4 = T_5 = T_{env}$ with T_{env} the temperature of the surrounding environment ($T_{env} = 150$ K and 200 K for the two measurements), $T_3 - T_4 = T_c - T_d = \Delta T_{cd}$, and $V_6 - V_1 = V_m$, we obtain

$$V_m = S_m \Delta T_{cd} = -(S_{Ni/Au} - S_{AuGe})\Delta T_{cd}. \quad (2)$$

Note that we are also considering connection lines with identical absolute thermoelectric powers.

From Eq. (2), the Seebeck coefficient of the $Au_{19.5}Ge_{80.5}$ thin film is given by

$$S_{AuGe} = S_m + S_{Ni/Au}. \quad (3)$$

The measured S_m is actually the relative Seebeck coefficient, including the contribution of the $Au_{19.5}Ge_{80.5}$ alloy and of the Ni/Au thin films used to realize the electrical probes on the alloy. Note that the long annealing step that ends the fabrication procedure is likely to induce Ni impurities in the Au contact probes. It has been shown that Fe magnetic impurities [36] or induced vacancies [37] can change the thermopower of Au, particularly at low temperatures (in the 1–100 K range), where its value can be inverted in sign while remaining at a few $\mu V/K$ in amplitude. On the contrary the high-temperature behavior (in the >100 K range) is only poorly affected. Given the temperature values at which we perform our measurements, we consider that our results should not be affected by the presence of magnetic impurities in the gold contacts. Anyway, even if such a contribution plays a role, it should not completely modify our conclusions. We can also make a rough estimation of the $S_{Ni/Au}$ contribution, by neglecting Ni diffusion in Au and by considering the Ni-Au contact as a simple bilayer structure. The Seebeck coefficient of the bilayer consisting of a 300-nm-thick Au layer on top of a 10-nm-thick Ni layer can be expressed in this case as $S_{Ni/Au} = S_{Au} + S_{Ni}(\rho_{Au}/\rho_{Ni})(d_{Ni}/d_{Au})$, where S_{Ni} is the Ni Seebeck coefficient, S_{Au} is the Au Seebeck coefficient, ρ_i and d_i ($i = \mathrm{Au, Ni}$) are the resistivity and thickness of the two layers. The difference in resistivity and thickness of the Ni and Au layers implies a contribution of S_{Ni} at 0.8% of the total value of $S_{Ni/Au}$. The value of S_{Ni} for the bulk case at room temperature is of the order of approximately -20 μV/K [38–40], and it reduces to approximately -8.4 μV/K and approximately -11 μV/K at $T = 150$ K and $T = 200$ K, respectively [41,42]. As a consequence, the correction to the value of $S_{Ni/Au}$ due to S_{Ni} becomes of the order of -0.07 μV/K and -0.09 μV/K at $T = 150$ K and $T = 200$ K, respectively. Note that this represents an overestimation, the Seebeck coefficient being expected to decrease in the thin-film limit with respect to the bulk case. By following Ref. [43], where the authors use equivalent fabrication techniques, the contribution of S_{Au} to $S_{Ni/Au}$ can be considered equal to $\simeq$1.02 μV/K at $T_{env} = 150$ K and to $\simeq$ 1.34 μV/K at 200 K [44,45]. By taking these corrections into account, we calculate that $S_{Ni/Au} = 0.95$ μV/K at $T = 150$ K and $S_{Ni/Au} = 1.25$ μV/K at $T = 200$ K. Within these assumptions, we can estimate, for the $Au_{19.5}Ge_{80.5}$ thin-film alloy, a Seebeck coefficient S_{AuGe} equal to 1.02 μV/K at $T_{env} = 150$ K and to 1.47 μV/K at $T_{env} = 200$ K.

Independent of the correct estimation of the contribution of the Ni-Au contacts, our experimental findings support the idea that 19.5% of the Au in the Au_xGe_{1-x} thin-film alloy induces thermoelectric properties that are comparable to that of simple Au.

It is known that intrinsic Ge has a high thermoelectric power, in the range of 100 μV $-$ 1 mV [46], the absolute value of which can be reduced by doping (n or p type) [46]. A net reduction of the absolute value of the Seebeck coefficient has already been measured in other systems showing a MIT, close to the transition conditions, such as VO_2 single crystals [47,48] and thin films [49,50] and $CuCr_{1-x}Fe_xS_2$ and $Cu_{1-x}Fe_xCrS_2$ powders [51]. In general, the thermopower is expected to vary significantly in such systems due to the changes in the electronic structure of the material across the MIT. One possible reason for the reduction in S is the formation of separate metallic and semiconducting domains inside the alloy and the way in which such domains become connected. Given the composition and the structural characterization of the $Au_{19.5}Ge_{80.5}$ alloy that we are studying, we can expect the formation of small metallic domains distributed in a matrix of larger semiconducting ones. The size and distribution of such domains are uncontrolled parameters and, depending on the particular configuration, they can be connected in series or parallel. The total absolute value of S is a complicated function in multiphase materials: it can be approximated by the sum of the different domain contributions weighted by their effective volume fraction and conductivity. Following Katase *et al.* [50], in a series connection scheme, $|S|$ can be expressed by $|S| = x|S|_M + (1-x)|S|_I$, where x is the volume fraction of metallic-on-insulating domains and $|S|_{M(I)}$ is the absolute thermopower of the metallic (insulating) domains, while in a parallel connection scheme the expression of the absolute thermopower reads $|S| = [x\sigma_M|S|_M + (1-x)\sigma_I|S|_I]/[x\sigma_M + (1-x)\sigma_I]$, where $\sigma_M(I)$ is the conductivity of the metallic (insulating) component. A substantial $|S|$ reduction is expected particularly in the presence of metallic percolation paths in the whole structure, promoting a parallel connection between domains of different nature. In such a configuration, while the total conductivity σ depends on the complete composition of the thin-film alloy, S is more sensitive to the metallic phase present in the alloy than to the insulating phase. This scheme, already proposed for VO_2 thin films [49,50], is particularly well suited in our case, where the multilayer fabrication procedure of the Au_xGe_{1-x} thin-film alloy could highly promote the presence of percolation paths.

Our findings demonstrate that the realized $Au_{19.5}Ge_{80.5}$ thin-film alloy presents thermoelectric properties similar to those of gold, with a low Seebeck coefficient, while retaining the characteristics of a good thermal sensor, making it very suitable for thermoelectric applications at the nanoscale. In particular, as mentioned at the beginning of this section, in the low-temperature limit the thin-film alloy shows no measurable thermoelectric signal and we find very low thermoelectric contributions in a higher temperature range, 150–200 K. This experimental observation, coupled to the measured temperature behavior of the resistivity, shows that the film has the right properties (a high-resistance temperature coefficient and a low Seebeck coefficient) to find application as a thermosensor for temperatures ranging from approximately a few kelvins to 200 K.

Here, we emphasize that in order to be used in molecular junctions, the Au_xGe_{1-x} alloy must fulfill another requirement: contacting molecular layers without forming short circuits. To achieve this, we have realized cross-bar molecular junctions by direct evaporation of an Au_xGe_{1-x} thin-film alloy on large-area molecular layers using three different molecules, namely bisthienylbenzene (BTB), nitrobenzene (NB), and anthraquinone (AQ). Their aromatic nature allows to graft them onto a metallic surface following the approach of electroreduction of diazonium salt. The molecular layers, with a 5–10 nm thickness, are grafted onto a 20 μm-width, 10 mm-long, 50 nm thick Au film following the method detailed in Refs. [18], [19], and [52]. We then evaporate the Au_xGe_{1-x} thin-film alloy directly on the molecular layer through an optical-lithography-defined mask. The realization of the alloy follows exactly the procedure described in Sec. II, where the low evaporation rates and the relatively low temperature used to promote the diffusion process of Au in Ge are particularly well suited for the presence of a molecular layer. By contacting the Au_xGe_{1-x} alloy with two Ni-Au electrodes, we finally end up with a large-area molecular junction with a vertical configuration, where the molecular layer is embedded between an Au contact and an Au_xGe_{1-x} contact.

Figures 5(a)–5(c) show the measured current-voltage (I-V) characteristics of the junctions realized with the different molecules BTB (red dots), NB (blue dots), and AQ (green dots). The I-V curves are measured by standard dc techniques by applying a fixed voltage on one of the junction electrodes, while measuring the current passing through a current-voltage amplifier. The three I-V curves, measured at $T = 2$ K, display the typical nonlinear behavior observed in molecular junctions [18,52–56]. The voltage range and maximum measured currents vary among the junctions due to the different nature of the molecular layer and to slight variation of the thickness of the molecular layer. The insets of Figs. 5(a)–5(c) show the log-log plots of the temperature dependence of the Au_xGe_{1-x} top electrode resistance in the temperature range $2\,\text{K} \leq T \leq 200\,\text{K}$ for the different molecular layers (same color code): the alloy atomic composition is also indicated. In all cases, the resistance behavior demonstrates a high sensitivity over the whole explored temperature range. Note also that, as shown in Fig. 2(b), despite slight variations in the alloy composition, the resistance of the top contact electrode remains strongly temperature dependent.

All of these results constitute a first step toward the measurement of the thermoelectric properties of large-area thin molecular layers. The realization of thermoelectric measurements across a molecular layer requires the ability to create a controlled temperature gradient across the layer, to measure such a gradient simultaneously, and to be sure

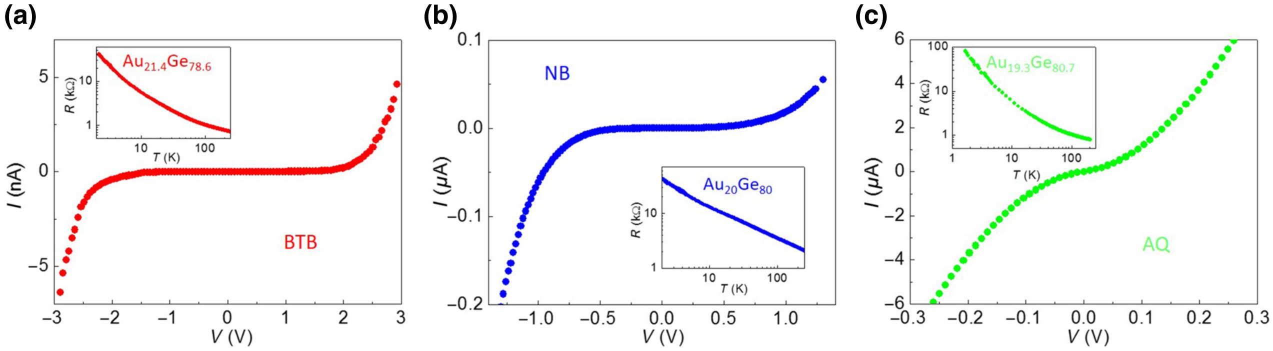

FIG. 5. The current-voltage (I-V) characteristics at $T = 2$ K of junctions including a molecular layer, namely BTB (a), NB (b), and AQ (c), and having an Au_xGe_{1-x} electrode. All I-V curves show the typical nonlinear behavior of molecular junctions. Insets: the temperature dependence of the resistance of the top electrodes realized with an Au_xGe_{1-x} thin-film alloy of each large-area molecular junction.

that the electrodes do not dominate the thermoelectric signal. Here, we demonstrate not only that the Au_xGe_{1-x} alloy is a suitable material for heating and temperature sensing, but also that due to its low Seebeck coefficient, it can be employed at the nanoscale without introducing spurious dominating thermoelectric signals. In any event, an accurate measurement of the temperature gradient across a molecular junction is still lacking. In particular, further implementations of additional local electrodes for temperature sensing at the top and bottom contacts of the junctions are required. These points are the focus of our current work.

IV. CONCLUSION

By using a nonlocal heating configuration scheme, we realize the thermoelectric characterization of Au_xGe_{1-x} thin-film alloys, close to the metal-insulator transition. Based on finite-element simulations and by taking all spurious thermoelectric effects into account, we reveal a Seebeck coefficient of the thin-film alloy with $x = 19.5\%$ very close to that of Au thin films. Simultaneously, we observe good electrical properties of the thin-film alloy, allowing it to be used as a high-resolution thermometer. Finally, we demonstrate the possibility of integrating such an element as the top electrode of a large-area vertical molecular junction, embedding thin (5–10 nm) molecular layers.

The performed detailed characterization suggests that Au_xGe_{1-x} thin-film alloys close to the metal-insulator transition allow the simultaneous realization of a local heater and thermometer, suggesting possible engineering solutions for thermoelectric applications at the nanoscale, such as the study of the thermoelectric properties of nanometric organic layers.

ACKNOWLEDGMENTS

This work has been funded partly by the Agence Nationale de la Recherche (ANR) (Project Remind, Grant No. ANR-15-CE09- 0001-02) and by the PE-01-2017 project of the Labex SEAM. The Commissariat Général à l’Investissement d’avenir (CGI) and the ANR are also acknowledged for their financial support. We acknowledge Dr. P. Martin for the electrografting of the molecular layer, Professor C. Goupil for useful discussions, and C. Manquest, P. Filloux, and S. Suffit for technical support within the cleanroom of the Laboratoire Matériaux et Phénomènes Quantiques (UMR 7162) at the University Paris Diderot.

[1] T. E. Humphrey, and H. Linke, Reversible Thermoelectric Nanomaterials, Phys. Rev. Lett. **94**, 096601 (2005).

[2] F. L. Bakker, J. Flipse, and B. J. van Wees, Nanoscale temperature sensing using the Seebeck effect, J. Appl. Phys. **111**, 084306 (2012).

[3] P. Reddy, S.-Y. Jang, R. A. Segalman, and A. Majumdar, Thermoelectricity in molecular junctions, Science **315**, 1568 (2007).

[4] A. Tan, S. Sadat, and P. Reddy, Measurement of thermopower and current-voltage characteristics of molecular junctions to identify orbital alignment, Appl. Phys. Lett. **96**, 013110 (2010).

[5] J. R. Widawsky, P. Darancet, J. B. Neaton, and L. Venkataraman, Simultaneous determination of conductance and thermopower of single molecule junctions, Nano Lett. **12**, 354 (2012).

[6] K. Baheti, J. A. Malen, P. Doak, P. Reddy, S.-Y. Jang, T. Don Tilley, A. Majumdar, and R. A. Segalman, Probing the chemistry of molecular heterojunctions using thermoelectricity, Nano Lett. **8**, 715 (2008).

[7] Y. Kim, W. Jeong, K. Kim, W. Lee, and P. Reddy, Electrostatic control of thermoelectricity in molecular junctions, Nat. Nanotech. **9**, 881 (2014).

[8] L. Cui, R. Miao, K. Wang, D. Thompson, L. A. Zotti, J. C. Cuevas, E. Meyhofer, and P. Reddy, Peltier cooling in molecular junctions, Nat. Nanotech. **13**, 122 (2018).

[9] M. Tsutsui, T. Morikawa, Y. He, A. Arima, and M. Taniguchi, High thermopower of mechanically stretched single-molecule junctions, Sci. Rep. **5**, 11519 (2015).

[10] J. P. Bergfield and C. A. Stafford, Thermoelectric signatures of coherent transport in single-molecule heterojunctions, Nano Lett. **9**, 3072 (2009).

[11] J. P. Bergfield, M. A. Solis, and C. A. Stafford, Giant thermoelectric effect from transmission supernodes, ACS Nano **4**, 5314 (2010).

[12] R. Miao, H. Xu, M. Skripnik, L. Cui, K. Wang, K. G. L. Pedersen, M. Leijnse, F. Pauly, K. Wärnmark, E. Meyhofer, P. Reddy, and H. Linke, Influence of quantum interference on the thermoelectric properties of molecular junctions, Nano Lett. **18**, 5666 (2018).

[13] A. J. Bergren, R. L. McCreery, S. R. Stoyanov, S. Gusarov, and A. Kovalenko, Electronic characteristics and charge transport mechanisms for large area aromatic molecular junctions, J. Phys. Chem. C **114**, 15806 (2010).

[14] J. Ru, B. Szeto, A. Bonifas, and R. L. McCreery, Microfabrication and integration of diazonium-based aromatic molecular junctions, ACS Appl. Mater. Interfaces **2**, 3693 (2010).

[15] A. M. Mahmoud, A. J. Bergren, N. Pekas, and R. L. McCreery, Towards integrated molecular electronic devices: Characterization of molecular layer integrity during fabrication processes, Adv. Funct. Mater. **21**, 2273 (2011).

[16] H. Yan, A. J. Bergren, and R. L. McCreery, All-carbon molecular tunnel junctions, J. Am. Chem. Soc. **133**, 19168 (2011).

[17] A. Bergren, K. Harris, F. Deng, and R. L. McCreery, Molecular electronics using diazonium-derived adlayers on carbon with Cu top contacts: Critical analysis of metal oxides and filaments, J. Phys. Condens. Matter **20**, 374117 (2008).

[18] P. Martin, M. L. Della Rocca, A. Anthore, P. Lafarge, and J.-C. Lacroix, Organic electrodes based on grafted

oligothiophene units in ultrathin, large-area molecular junctions, J. Am. Chem. Soc. **134**, 154 (2012).

[19] Q. V. Nguyen, P. Martin, D. Frath, M. L. Della Rocca, F. Lafolet, C. Barraud, P. Lafarge, V. Mukundan, D. James, R. L. McCreery, and J.-C. Lacroix, Control of rectification in molecular junctions: Contact effects and molecular signature, J. Am. Chem. Soc. **139**, 11913 (2017).

[20] L. Cui, R. Miao, C. Jiang, E. Meyhofer, and P. Reddy, Perspective: Thermal and thermoelectric transport in molecular junctions, J. Chem. Phys. **146**, 092201 (2017).

[21] B. W. Dodson, W. I . McMillan, J. M. Mochel, and R. C. Dynes, Metal-Insulator Transition in Disordered Germanium-Gold Alloys, Phys. Rev. Lett. **46**, 46 (1981).

[22] M. Osofsky, H. Tardy, M. LaMadrid, and J. M. Mochel, DC conductivity of strong and weak electron spin-orbit scattering materials near the metal-insulator transition, Phys. Rev. B **32**, 2101 (1985).

[23] M. Osofsky, J. B. Bieri, M. LaMadrid, W. Contrata, and J. M. Mochel, Electrical field effects near the metal-insulator transition, Phys. Rev. B **38**, 12215 (1988).

[24] D.-M. Zhu and F. Lin, Fabrication of Ge-Au film thermometers using interfacial atomic diffusion, Rev. Sci. Instrum. **64**, 2624 (1993).

[25] Y. M. Brovman, J. P. Small, Y. Hu, Y. Fang, C. M. Lieber, and P. Kim, Electric field effect thermoelectric transport in individual silicon and germanium/silicon nanowires, J. Appl. Phys. **119**, 234304 (2016).

[26] Y. M. Zuev, J. Seok Lee, C. Galloy, H. Park, and P. Kim, Diameter dependence of the transport properties of antimony telluride nanowires, Nano Lett. **10**, 3037 (2010).

[27] Y. Tian, M. R. Sakr, J. M. Kinder, D. Liang, M. J. MacDonald, R. L. J. Qiu, H.-J. Gao, and X. P. A. Gao, One-dimensional quantum confinement effect modulated thermoelectric properties in InAs nanowires, Nano Lett. **12**, 6492 (2012).

[28] J. Moon, J.-H. Kim, Z. C. Y. Chen, J. Xiang, and R. Chen, Gate-modulated thermoelectric power factor of hole gas in Ge-Si core-shell nanowires, Nano Lett. **13**, 1196 (2013).

[29] Y. M. Zuev, W. Chang, and P. Kim, Thermoelectric and Magnetothermoelectric Transport Measurements of Graphene, Phys. Rev. Lett. **102**, 096807 (2009).

[30] S. G. Nam, D. K. Ki, and H. J. Lee, Thermoelectric transport of massive Dirac fermions in bilayer graphene, Phys. Rev. B **82**, 245416 (2010).

[31] J. P. Small, K. M. Perez, and P. Kim, Modulation of Thermoelectric Power of Individual Carbon Nanotubes, Phys. Rev. Lett. **91**, 256801 (2003).

[32] T. Kodama, M. Ohnishi, W. Park, T. Shiga, J. Park, T. Shimada, H. Shinohara, J. Shiomi, and K. E. Goodson, Modulation of thermal and thermoelectric transport in individual carbon nanotubes by fullerene encapsulation, Nat. Mater. **16**, 892 (2017).

[33] E. J. Koop, M. J. Iqbal, F. Limbach, M. Boute, B. J. van Wees, D. Reuter, A. D. Wieck, B. J. Kooi, and C. H. vanderWal, On the annealing mechanism of AuGe/Ni/Au ohmic contacts to a two-dimensional electron gas in GaAs/$\mathrm{Al}_x\mathrm{Ga}_{1-x}$As heterostructures, Semicond. Sci. Technol. **28**, 025006 (2013).

[34] N. A. Fortune, M. J. Graf, and K. Murata, Physical dependence of the sensitivity and room-temperature stability of $\mathrm{Au}_x\mathrm{Ge}_{1-x}$ thin film resistive thermometers on annealing conditions, Rev. Sci. Instr. **69**, 133 (1998).

[35] A. Miyata, M. Abe, Y. Okamoto, T. Kawahara, J. Morimoto, and N. Inoue, Thermoelectric properties of amorphous Ge/Au and Si/Au thin films, IEEJ Trans. FM **124**, 307 (2004).

[36] N. Wendling, J. Chaussy, and J. Mazuer, Thin gold wires as reference for thermoelectric power measurements of small samples from 1.3 to 350 K, J. Appl. Phys. **73**, 2878 (1993).

[37] P. P. Huebener, Thermoelectric power of lattice vacancies in gold, Phys. Rev. **135**, A1281 (1964).

[38] A. T. Burkov, A. Heinrich, P. P. Konstantinov, T. Nakama, and K. Yagasaki, Experimental set-up for thermopower and resistivity measurements at 100–1300 K, Meas. Sci. Technol. **12**, 264 (2001).

[39] V. Ponnambalam, S. Lindsey, N. S. Hickman, and T. M. Tritt, Sample probe to measure resistivity and thermopower in the temperature range of 300–1000 K, Rev. Sci. Instr. **77**, 073904 (2006).

[40] L. Abadlia, F. Gasser, K. Khalouk, M. Mayoufi, and J. G. Gasser, New experimental methodology, setup and Labview program for accurate absolute thermoelectric power and electrical resistivity measurements between 25 and 1600 K: Application to pure copper, platinum, tungsten, and nickel at very high temperatures, Rev. Sci. Instr. **85**, 095121 (2014).

[41] R. D. Park and R. Orbach, in *Thermoelectricity in metallic conductors*, edited by F. J. Blatt and P. A. Schroeder (Springer, New York, 1978), p.281.

[42] F. J. Blatt, P. A. Schroeder, C. L. Foiles, and D. Greig, *Thermoelectric power of metals* (Premium Press, New York, 1976).

[43] W. Kim, J. Zide, A. Gossard, D. Klenov, S. Stemmer, A. Shakouri, and A. Majumdar, Thermal Conductivity Reduction and Thermoelectric Figure of Merit Increase by Embedding Nanoparticles in Crystalline Semiconductors, Phys. Rev. Lett. **96**, 045901 (2006).

[44] N. Cusack and P. Kendall, The absolute scale of thermoelectric power at high temperature, Proc. Phys. Soc. **72**, 898 (1958).

[45] D. M. Rowe, *CRC Handbook of Thermoelectrics*, edited by D. M. Rowe (CRC Press, Boca Raton, 1995).

[46] T. H. Geballe and G. W. Hull, Seebeck effect in germanium, Phys. Rev. **94**, 1134 (1954).

[47] J. Cao, W. Fan, H. Zheng, and J. Wu, Thermoelectric Effect across the Metal-Insulator Domain Walls in VO_2 Microbeams, Nano Lett. **9**, 4001 (2009).

[48] Y. Gu, J. Cao, J. Wu, and L.-Q. Chen, Thermodynamics of strained vanadium dioxide single crystals, J. Appl. Phys. **108**, 083517 (2010).

[49] D. Fu, K. Liu, T. Tao, K. Lo, C. Cheng, B. Liu, R. Zhang, H. A. Bechtel, and J. Wu, Comprehensive study of the metal-insulator transition in pulsed laser deposited epitaxial VO_2 thin films, J. Appl. Phys. **113**, 043707 (2013).

[50] T. Katase, K. Endo, and H. Ohta, Thermopower analysis of metal-insulator transition temperature modulations in vanadium dioxide thin films with lattice distortion, Phys. Rev. B **92**, 035302 (2015).

[51] E. V. Korotaev, M. M. Syrokvashin, I. Yu. Filatova, K. G. Pelmenev, V. V. Zvereva, and N. N. Peregudova, Seebeck Coefficient of Cation-Substituted Disulfides $\mathrm{CuCr}_{1-x}\mathrm{Fe}_x\mathrm{S}_2$ and $\mathrm{Cu}_{1-x}\mathrm{Fe}_x\mathrm{CrS}_2$, J. Electron. Mater. **47,** 3392 (2018).

[52] V. Rabache, J. Chaste, P. Petit, M. L. Della Rocca, P. Martin, J.-C. Lacroix, R. L. McCreery, and P. Lafarge, Direct observation of large quantum interference effect in anthraquinone solid-state junctions, J. Am. Chem. Soc. **135,** 10218 (2013).

[53] Z. Xie, I. Baldea, C. E. Smith, Y. Wu, and C. D. Frisbie, Experimental and theoretical analysis of nanotransport in oligophenylene dithiol junctions as a function of molecular length and contact work function, ACS Nano **9,** 8022 (2015).

[54] A. P. Bonifas and R. L. McCreery, Assembling molecular electronic junctions one molecule at a time, Nano Lett. **11,** 4725 (2011).

[55] H. Yan, A. J. Bergren, R. McCreery, M. L. Della Rocca, P. Martin, P. Lafarge, and J.-C. Lacroix, Activationless charge transport across 4.5 to 22 nm in molecular electronic junctions, Proc. Natl. Acad. Sci. U.S.A. **110**, 5326 (2013).

[56] A. Vilan, D. Aswal, and D. Cahen, Large-area, ensemble molecular electronics: Motivation and challenges, Chem. Rev. **117**, 4248 (2017).